Journal of Materials Chemistry A

Accepted Manuscript

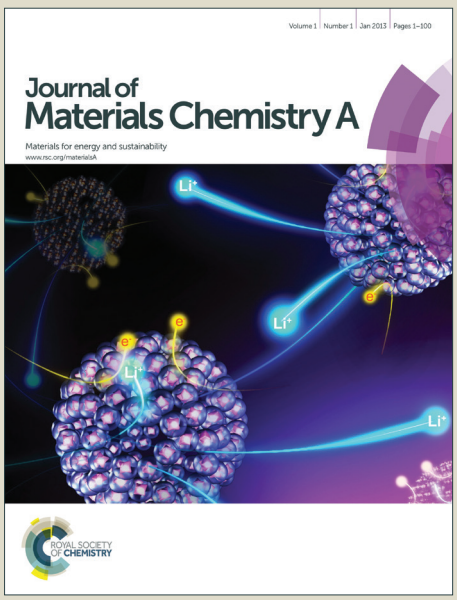

ROYAL SOCIETY OF CHEMISTRY

www.rsc.org/materialsA

Mesoporous $CuCo_2O_4$ nanograss as multi-functional electrodes for supercapacitors and electro-catalysts

Jinbing Cheng[†a,b], Hailong Yan[†a,b], Yang Lu[†a,b,c], Kangwen Qiu[†a,b], Xiaoyi Hou[a,b], Jinyou Xu[a,b], Lei Han[a], Xianming Liu[d], Jang-Kyo Kim[e] and Yongsong Luo[*a,b]

[a]*School of Physics and Electronic Engineering, Xinyang Normal University, Xinyang 464000, P. R. China.*

[b]*Key Laboratory of Advanced Micro/Nano Functional Materials, Xinyang Normal University, Xinyang 464000, P. R. China.*

[c]*School of Material Science and Engineering, Hebei University of Technology, Tianjin 300130, P. R. China.*

[d]*College of Chemistry and Chemical Engineering, Luoyang Normal University, Luoyang 471022, P. R. China.*

[e]*Department of Mechanical and Aerospace Engineering, The Hong Kong University of Science and Technology, Clear Water Bay, Kowloon, Hong Kong, P. R. China.*

Abstract

Hierarchical, mesoporous $CuCo_2O_4$ nanograss has been synthesized on copper foam using a simple and cost-effective hydrothermal approach followed by a post-annealing treatment. The electrodes made from the novel nanoarchitecture exhibit multi-functional electrochemical performance. They deliver an excellent specific capacitance of 796 F g^{-1} at a current density of 2 A g^{-1} in a 2 M KOH aqueous solution and a long-term cyclic stability of 94.7% capacitance retention after 5000 cycles. When applied to electro-catalytic oxidation of methanol, the current density of the $CuCo_2O_4$/Cu foam electrode in 1 M KOH mixed with 0.5 M methanol is maintained up to 27.6 A g^{-1}. The superior electrochemical performances are mainly due to the unique one dimensional porous acicular architecture with very large surface area and

* To whom correspondence should be addressed: E-mail: ysluo@xynu.edu.cn

† These authors contribute equally to this work.

porosity grown on highly conductive Cu substrate, offering faster ion/electron transfer, an improved reactivity and an enhanced structural stability. The fabrication strategy presented here is simple, cost-effective and scalable, which can open new avenues for large-scale applications of the novel materials in energy storage.

Keywords: Supercapacitor; Electro-catalytic; Energy storage; Copper foam; Mesoporous

1. Introduction

Efficient energy storage and its economic use are central to the development of modern communication networks, transportation systems and medical devices.[1-3] Supercapacitors can offer higher power densities with longer cyclic lifespans than rechargeable batteries, and store higher energy densities than conventional capacitors,[4-8] thus have been considered one of the most promising next-generation energy storage devices. On the other hand, the rapid depletion of fossil fuel and ever-growing environmental problems have aroused widespread attention in developing and designing novel materials for energy conversion devices, like fuel cells.[9-11] Direct methanol fuel cells (DMFCs) are regarded a potential candidate for power generation in electric vehicles.[12] This stems from the facts that methanol is a relatively high energy density fuel, it is liquid at ambient temperature, is of low cost and available at industrial scale and the infrastructures for production and distribution are already available.[13] Direct methanol fuel cells, as a member of fuel cells, have attracted considerable interest due to abundant raw materials, low operating temperatures as well as low pollution. It is widely accepted that the relatively low activity and high cost are the two main obstacles inhibiting the applications of

supercapacitors and DMFCs.[14] Thus, the exploration of new electrode materials, including noble and non-noble metals, is necessary for performance improvements.[15]

Transition metal based composite materials exhibit synergistic enhancements in properties like chemical activity, stability and resistance to poisoning[16] for both supercapacitors and catalytic activities, which are much better than a simple combination of individual components. Important properties of electrode materials include the morphology, size, surface area, porosity and pore size distribution, etc. In particular, hierarchical porous nanostructures deposited directly on conductive metal substrates containing large surface areas are highly desirable for efficient energy storage and conversion due to their short transport pathways for electrons and ions.[17,18] Among the various electrode materials, spinel copper cobaltite ($CuCo_2O_4$) has been widely used as a very promising electrode for supercapacitors,[19,20] catalysts,[21] and Li-ion batteries[22] because it offers many advantages, such as low-cost, abundant resources and environmentally friendly. More significantly, $CuCo_2O_4$ possesses a higher electrochemical activity as well as a much better electronic conductivity, at least two orders of magnitude higher, than the individual components, copper oxides and cobalt oxides, acting alone.[23] Nevertheless, few attempts have been reported to date regarding its application as supercapacitor.

This paper reports the synthesis of novel hierarchical, mesoporous $CuCo_2O_4$ nanograss coating on copper foam based on a facile hydrothermal process followed by post-annealing treatment. The nanograsses consist of a myriad of nanoscale acicular leaves that are interconnected through the highly conductive Cu foam substrate,

offering an intricate transportation network for fast ion and electron transport. Their attractive electrochemical performances as the electrodes for supercapacitors as well as electro-catalytic oxidation of methanol are demonstrated. The hierarchical, mesoporous $CuCo_2O_4$ electrodes manifest ultrahigh capacitance, electro-catalytic activity and excellent cyclic stability at high rates.

2. Experimental

2.1 Synthesis of mesoporous $CuCo_2O_4$ nanograss arrays

All the reagents were analytical grade and directly used without further purification. Prior to deposition, copper foams (90 pores per inch, 650 g m^{-2} surface density, and about 2.5 mm thick) of 1.5 cm × 4.0 cm in rectangular shape were cleaned by sonication in acetone, 1 M HCl solution, deionized (DI) water, and ethanol for 15 min each. Nanograss was grown on copper foam via a simple one-pot hydrothermal process. 1 mmol (0.24 g) of $Cu(NO_3)_2{\cdot}3H_2O$ and 2 mmol (0.58 g) of $Co(NO_3)_2{\cdot}6H_2O$ were dissolved into 35 mL of DI water and 5 mL of ethanol absolute, followed by the addition of 15 mmol (0.90 g) of urea at room temperature, and the mixture was stirred to form a clear blue solution. Then the mixture was transferred into a 50 mL Teflon-lined stainless steel autoclave. The cleaned Cu foam was immersed in the mixture, and the autoclave was kept at 120 ^{o}C for 12 h. After cooling down to room temperature, the Cu foam was taken out and washed with DI water and ethanol several times to obtain Cu-Co hydroxide precursor on its surface. The as-prepared precursor was annealed at 400 ^{o}C in air for 4 h at a ramping rate of 1 ^{o}C min^{-1} to obtain nanograss-shaped $CuCo_2O_4$.

2.2 Materials characterization

The crystalline structure and phase purity of the products were identified by X-ray diffraction (XRD) analysis on a D8 Advance (Bruker) automated X-ray diffractometer system with Cu-Kα (λ = 1.5418 Å) radiation at 40 kV and 40 mA, and 2θ ranging from 10° to 80° at room temperature. Raman spectroscopy was carried out using an INVIA Raman microprobe (Renishaw Instruments) with a 532 nm laser source and a 50×objective lens. The morphologies and structures were examined on a field emission scanning electron microscope (FESEM, JEOL S-4800) and a transmission electron microscope (TEM, JEOL JEM-2010). The elemental analysis was carried out using an energy-dispersive X-ray spectroscope (EDS, Bruker-QUANTAX) attached to the FESEM. The Brunauer-Emmett-Teller (BET) surface areas of the electrode materials of 20 mg in weight were determined using the nitrogen sorption/desorption isotherms obtained at 77K from a surface area and porosity analyzer (Quadrasorb SI-MP, Quantachrome). The chemical elements of the electrodes were analyzed on a X-ray photoelectron spectroscopy (XPS, Perkin-Elmer PHI 5600 XPS system) with a resolution of 0.3~0.5 eV from a monochromated aluminum anode X-ray source.

2.3 Measurement of electrochemical performance of supercapacitor

The electrochemical properties of $CuCo_2O_4$ electrodes were studied based on cyclic voltammetry (CV), electrochemical impedance spectroscopy (EIS) tests and galvanostatic charge/discharge (GCD) curves using three-electrode cells on a electrochemical workstation (CHI 660E). The three-electrode cell contained a Pt foil as the counter electrode, a Hg/HgO as the reference electrode and $CuCo_2O_4$ (~4 mg

cm^{-2}) grown on copper foam as the working electrode, with a solution of 2 M KOH as the electrolyte. The CV analysis was performed between 0 and 0.6 V *vs.* Hg/HgO at scan rates ranging from 5 to 50 mV s^{-1}. The GCD tests were conducted in a stable potential window between 0 and 0.6 V at different current densities of 2-10 A g^{-1} on a LAND battery program-control test system. The EIS measurements were made by applying an AC voltage with 10 mV amplitude in a frequency range from 0.01 Hz to 100 kHz. The nominal area of $CuCo_2O_4$ electrodes immersed into the electrolyte was controlled to be around 1.0 cm × 2.0 cm. The specific capacitance, C (F g^{-1}), was calculated according to the following equation:

$$C = \frac{I\Delta t}{M\Delta v} \tag{1}$$

where I (mA) represents the discharge current, and M (mg), ΔV (v) and Δt (s) designate the mass of active material, potential drop during discharge and total discharge time, respectively.

2.4 Measurement of electro-catalytic performance

The electro-catalytic properties of $CuCo_2O_4$ electrodes were measured by cyclic voltammetry (CV), chronoamperometry (CA) and electrochemical impedance spectroscopy (EIS) tests carried out at room temperature. The electro-catalytic activities of the $CuCo_2O_4$ electrodes for oxidation of methanol were investigated on a CHI660E electrochemical workstation. A standard three-electrode system was employed which consisted of a $CuCo_2O_4$ working electrode, a Pt foil counter electrode and a Hg/HgO reference electrode. Solutions containing 1 M KOH without and with 0.5 M methanol were used as the electrolytes.

3. Results and Discussions

3.1 Morphology and structure of $CuCo_2O_4$

The crystallographic phase of the $CuCo_2O_4$ was identified by XRD, and the typical wide-angle diffraction patterns are shown in Fig. 1. They consisted of nine well-defined diffraction peaks that can be indexed into a cubic spinel $CuCo_2O_4$ crystalline structure (JCPDF card No. 78-2177).[22] In general, the coexistence of Co and Cu in the oxide favors the formation of $CuCo_2O_4$.[24] The composition and structure of the $CuCo_2O_4$ were further confirmed by Raman analysis, as shown in Fig. S1. Four prominent peaks were observed at 187, 479.1, 521.5 and 678.3 cm^{-1}, which are assigned to F_{2g}, E_g, F_{2g} and A_{1g} models of $CuCo_2O_4$, respectively. Only the Co-O and Cu-O vibrations were detected and signals from the OH group were absent, indicating that the precursor cobalt/copper metallic carbonate hydroxide salts were completely decomposed after calcination at 400 ^oC. These results are consistent with those reported previously.[19]

Fig. 2 gives the thermogravimetric and differential thermal analysis (TG-DTA) curves of the Cu-Co hydroxide precursor in air, showing the beginning of decomposition at ~210 ^oC after the evaporation of water and other small molecular species. In the DTA curve, there was a strong heat absorption peak at ~392 ^oC, originating from the decomposition of Cu-Co hydroxide to $CuCo_2O_4$. These results demonstrate that the annealing temperature, 400 ^oC, chosen in this study was appropriate.

The SEM images of $CuCo_2O_4$ taken at increasingly higher magnifications are

shown in Fig. 3. A coating of $CuCo_2O_4$ was uniformly grown over the whole skeleton of Cu foam (Fig. 3a). The higher magnification images (Fig. 3b, 3c) show that the $CuCo_2O_4$ coating consisted of intertwined nanostructured grasses, and the enlarged view (Fig. 3d) presents the nanograss comprised of a myriad of bundled, acicular leaves of less than 200 nm in diameter and ~2-3 μm in length. In light of these distinct morphological features, Fig. 4 illustrates the design and synthesis strategy of $CuCo_2O_4$ on Cu foam as an electrode material. The whole process involved two steps: firstly, the Cu-Co hydroxide precursor in the form of a nanograss coating was uniformly grown on the Cu foam via a facile, hydrothermal process; and secondly, $CuCo_2O_4$ was obtained after annealing in argon while maintaining the nanograss-shaped structure.

Detailed morphological and structural features of the $CuCo_2O_4$ nanograss were studied by TEM, HRTEM and selected-area electron diffraction (SAED). Fig. 5a reveals that the single $CuCo_2O_4$ nanoleaf consisted of numerous interconnected nanoparticles. The HRTEM image (Fig. 5b) presents that the lattice fringes were ~0.242 and 0.468 nm, corresponding to the (311) and (111) planes of spinel structured $CuCo_2O_4$, respectively.[25] The SAED pattern (Fig. 5c) shows well-defined diffraction rings, indicating the poly-crystalline nature of the cubic phase. These rings can be readily indexed to the (220), (311), (400) and (440) planes of the cubic $CuCo_2O_4$ phase, which are consistent with the above XRD results. The corresponding EDS spectrum (Fig. 5d) presents O, Co and Cu elements with the atomic ratio of Co to Cu being approximately 2:1.

The chemical compositions of $CuCo_2O_4$ are analyzed by XPS analysis, and the spectra are shown in Fig. S2. The general survey spectrum (Fig. S2a) indicates the presence of C, Cu, Co and O elements and the absence of other impurities. The Cu 2p deconvoluted spectrum (Fig. S2b) had two prominent $2p_{3/2}$ and $2p_{1/2}$ spin-orbit peaks at binding energies of 933.8 and 954.7 eV, and two shakeup satellites (identified as "Sat.").[26] Two major peaks at binding energies of 779.7 and 795.2 eV were observed from the complex Co 2p spectrum (Fig. S2c), corresponding to the Co $2p_{3/2}$ and Co $2p_{1/2}$ spin-orbit peaks, respectively. The O 1s detailed spectrum (Fig. S2d) was resolved into two components, centered at 530 and 531.3 eV, respectively, which are attributed to the O^{2-} forming oxide with Co and Cu elements, and OH^-.

The porous structure of $CuCo_2O_4$ nanograss needs further discussion because of the importance of pores and surface area as electrodes in supercapacitors. The porous structure enable facile transport of the electrolyte to the surface of $CuCo_2O_4$, resulting in rapid charge transfer reactions due to the shortened ion diffusion paths. It is thought that the annealing process helped the formation of pores within the individual leaves of $CuCo_2O_4$ nanograss arising from the release of the gas during the decomposition of Cu-Co hydroxide precursor. Fig. S3 shows type IV adsorption/desorption isotherms with type H3 hysteresis loops according to the IUPAC (International Union of Pure and Applied Chemistry) classifications of hysteresis loops,[27] a reflection of typical mesoporous microstructure.[28,29] After a steady increase, the adsorbed nitrogen volume surged at a relative pressure close to unity, implying the existence of large interconnected voids or void space within the nanograss. The pore size distribution

(PSD) data (inset of Fig. S3) show that the majority of the pores fell in the range of 3-8 nm, which is known to be optimal for supercapacitor applications. The mesoporous structure gave rise to a high porosity of 0.13 cm^3 g^{-1} and a large BET specific surface area of 109 m^2 g^{-1}.

3.2 Supercapacitor performance measurements

Potential sweep CV curves obtained at different scan rates shown in Fig. 6a present typical pseudocapacitive characteristics. In general, one pair of broadly and poorly defined redox peaks were observed in the CV plots, originating from the faradaic redox reactions related to M-O/M-O-OH, where M represents both the Cu and Co ions.[30-33] When the scan rate increased from 5 to 50 mV s^{-1}, the corresponding current enhanced while the shape of the CV curves remained largely unchanged, except for the shifts of the peak positions. Fig. S4 showed the CVs of the $CuCo_2O_4$ nanograss electrode in comparison with neat Cu foam electrode at a scan rate of 30 mV s^{-1}, the signal from the Cu foam electrode was negligible compared to the former. The galvanostatic charge-discharge curves obtained at different current densities at potentials between 0 and 0.6 V were shown in Fig. 6b. With increasing current density, without obvious IR (internal resistance) drops, the $CuCo_2O_4$ electrode exhibited outstanding electrochemical reversibility.

The $CuCo_2O_4$ electrode exhibited an excellent long-term cyclic stability evidenced by the very stable charge/discharge curves for the last 10 cycles among 5000 cycles (Fig. 6c). The charge/discharge curves for a given cycle were quite symmetrical against each other, indicating negligible structural change of the electrode during the

charge/discharge processes. Fig. 6d presents specific capacitance as a function of current density. At a relatively low current density of 2 A g^{-1}, the $CuCo_2O_4$ electrode delivered a high capacitance of 796 F g^{-1}; and when the current density was increased to 10 A g^{-1}, the capacitance was recorded at 611 F g^{-1} with ~76.8 % retention compared to that for 2 A g^{-1}. Correspondence between specific capacitances and capacities at different current densities were shown in Fig. S5. As can be seen, there was an excellent capacity value of 133 mA h g^{-1} at 2A g^{-1}.

The cycle stability of supercapacitors is a crucial parameter for their practical applications. The long-term stability of the $CuCo_2O_4$ electrode was examined at 2 A g^{-1} and 8 A g^{-1} and the results are shown in Fig. 7a. The capacitance retention of the electrode after 5000 cycles at 2 A g^{-1} s remarkable ~94.7% of the initial value, which is partly confirmed by the SEM image of the electrode taken ex situ after 5000 cycles (see inset) showing little structural changes. Moreover, the capacitance retention of the electrode is ~94% at the higher current density of 8 A g^{-1}, which also exhibits good cycle stability. The capacitances measured at different current densities shown in Fig. 7b further confirmed excellent high rate capabilities of the electrode. During the first 300 cycles at with a low current density of 2 A g^{-1}, the electrode presented very stable cyclic stability with a specific capacity as high as 796 F g^{-1}. Upon step-wise increases in charge/discharge rate in the following 1200 cycles, the electrode continued to demonstrate stable capacitances. With the current rate back to 2 A g^{-1} for the rest of cycles, a remarkable capacitance of ~790 F g^{-1} was recovered without any noticeable degradation, confirming excellent rate performance and cyclic

stability.

To further demonstrate the benefits of the $CuCo_2O_4$ nanograss electrode material, the EIS revealed excellent electronic conductivities of the electrode during the redox process. Nyquist plots in Fig. 7c were composed of an arc in the high frequency region and a linear line in the low frequency region. The semicircle of the Nyquist plot corresponds to the Faradic reactions and its diameter represents the interfacial charge transfer resistance (R_{ct}). The internal resistance (R_s) is the sum of the ionic resistance of the electrolyte, the intrinsic resistance of active material and the contact resistance at the active material/current collector interface,[34] and can be obtained from the intercept of the plots on the real axis. The inset of Fig. 7c gives an equivalent circuit used to fit the EIS curves to measure R_s and R_{ct}, where Z_w and CPE are the Warburg impendence and the constant phase element, respectively.[35] The results measured after 1 and 5000 cycles are shown in Table S1, where R_{ct} and R_s increased by 15% and less than 5%, indicating that although the charge transfer resistance increased to a certain extent, the internal resistance little deteriorated owing to a good contact between the nanograss electrode and the current collector with an excellent electrical conductivity. As the individual $CuCo_2O_4$ leaves were composed of nanocrystallites and mesopores, the transportation of electrolytes through their nanochannels was easy for efficient redox reactions during the Faradaic charge storage process. The direct growth of $CuCo_2O_4$ nanograss onto the highly conductive Cu foam substrate means participation of the majority of the highly porous electrode materials in the ultrafast electrochemical reaction, as schematically shown in Fig. 7d.

The above discussion suggests that the $CuCo_2O_4$ nanograss with appealing morphological and structural features can make promising, freestanding electrodes for high performance supercapacitors.

3.3 CH_3OH electro-oxidation performance for DMFCs

The methanol electro-oxidation performance of the $CuCo_2O_4$ electrode was investigated by CV, CA and EIS tests. Fig. 8a illustrates the CV plot of the $CuCo_2O_4$ electrode in 1 M KOH blank electrolyte at a scan rate of 5 mV s^{-1}. A pair of broad and strong redox peaks, marked as A and B, were observed, which originate mainly from the charge transfer processes of solid state redox. In order to eliminate the influence of Cu foam (CF), the electro-catalytic activities of the methanol oxidation on Blank/CF and $CuCo_2O_4$/CF electrodes were compared. The Blank/CF and $CuCo_2O_4$/CF electrodes showed different behaviors in 1 M KOH in the presence of 0.5 M methanol (Fig. 8b). The current of $CuCo_2O_4$/CF was much higher than that of Blank/CF, indicating the effect of blank CF on electro-catalytic oxidation of methanol can be ignored. The current densities of $CuCo_2O_4$/CF in 1 M KOH without and with 0.5 M methanol were 2.8 and 27.8 A g^{-1}, respectively. The corresponding catalytic mechanism for CH_3OH electro-oxidation on the $CuCo_2O_4$ electrode can be expressed in the following equations:[36-38]

$$CuCo_2O_4 + OH^- + H_2O - 3e^- \rightarrow CuOOH + 2CoOOH \quad (2)$$

$$CuOOH + CH_3OH + 1.25O_2 \rightarrow Cu(OH)_2 + CO_2 + 1.5H_2O \quad (3)$$

$$2CoOOH + 2CH_3OH + 2.5O_2 \rightarrow 2Co(OH)_2 + 2CO_2 + 3H_2O \quad (4)$$

EIS provides useful information on electron and charge transfer in fuel cell

reactions. EIS measurements were recorded at 0.5 and 0.6 V at a frequency range from 0.01 Hz to 10 kHz. Similar EIS results were observed at different potential (Fig. 8c). However, the diameter of the primary semicircle obtained at 0.6 V was much smaller than that at 0.5 V, implying faster reaction kinetics for methanol oxidation and a lower electron or charge transfer resistance at 0.6 V.[39-41] In other words, 0.6 V was more suitable for methanol electro-oxidation than 5 V.

CA is a useful tool to investigate the electrochemical stability of a catalyst. According to the EIS results, 0.6 V was selected as the optimal potential for investigating the stability of the Blank/CF and $CuCo_2O_4$/CF electrodes for methanol oxidation. As depicted in Fig. 8d, both eletrodes exhibited no distinct decay in 1000 s, demonstrating that the CF was an ideal supporter for catalyst in DMFCs and the $CuCo_2O_4$/CF was stable in methanol oxidation. Moreover, the current density (~24.5 A g^{-1}) of the $CuCo_2O_4$/CF electrode was almost 6 times higher than that (~4.12 A g^{-1}) of the Blank/CF electrode, confirming that the $CuCo_2O_4$/CF electrode had a much higher electro-catalytic activity of methanol oxidation while the effect of CF was negligible.

4. Conclusions

In summary, this paper presents a facile and highly-efficient hydrothermal method for direct growth of mosoporous nanograss-shaped $CuCo_2O_4$ coatings on Cu foam substrates. The synthesis route was robust and scalable so that the technique may be extended to fabricate other nanostructures for various applications in electrochemical energy storage and optical devices. The $CuCo_2O_4$ nanograss electrodes were tested to

demonstrate their multi-functionality, including their supercapacitor performance and electro-catalytic behavior in CH_3OH. Several unique structural features and ameliorating properties are considered responsible for the excellent electrochemical performance of the $CuCo_2O_4$ electrode. (i) The direct growth of freestanding $CuCo_2O_4$ nangrass on a highly conductive Cu foam substrate means total elimination of polymer binders and conductive additives, substantially reducing the "dead volume" in electrode. (ii) The direct growth also ensured outstanding mechanical adhesion and electrical connection to the current collector. (iii) The unique one dimensional porous acicular architecture with very large surface area and porosity, offering faster ion/electron transfer, an improved reactivity and an enhanced electrochemical kinetics. The desirable electro-catalytic performance clearly indicates that the mesoporous $CuCo_2O_4$ nanograss is a promising electrode material, demonstrating the potential of transition metal oxides in the development of high performance supercapacitors and DMFCs.

Acknowledgments

This work was financially supported by the National Natural Science Foundation of China (Nos. U1204501, U1304108 and 21373107), the Innovative Research Team (in Science and Technology) in University of Henan Province (No. 13IRTSTHN018) and University Students Sustentation Fund of Xinyang Normal University (No. 2014KYJJ30).

Notes and references

1 M. Armand and J. M. Tarascon, *Nature*, 2008, **451**, 652.

2 Y. S. Luo, J. S. Luo, J. Jiang, W. W. Zhou, H. P. Yang, X. Y. Qi, H. Zhang, H. J. Fan, Y. W. Y. Denis, C. M. Li and T. Yu, *Energy Environ. Sci*., 2012, **5**, 6559.

3 A. S. Arico, P. Bruce, B. Scrosati, J. M. Tarascon and W. V. Schalkwijk, *Nat. Mater*., 2005, **4**, 366.

4 Y. S. Luo, J. S. Luo, J. Jiang, W. W. Zhou, H. P. Yang, X. Y. Qi, H. Zhang, H. J. Fan, Y. W. Y. Denis, C. M. Li and T. Yu, *J. Mater Chem. A*, 2013, **1**, 273.

5 X. W. Lou, L. A. Archer and Z. C. Yang, *Adv. Mater*., 2008, **20**, 3987.

6 D. Z. Kong, J. S. Luo, Y. L. Wang, W. N. Ren, T. Yu, Y. S. Luo, Y. P. Yang and C. W. Cheng, *Adv. Funct. Mater*., 2014, **24**, 3815.

7 J. P. Liu, J. Jiang, C. W. Cheng, H. X. Li, J. X. Zhang, H. Gong and H. J. Fan, *Adv. Mater.*, 2011, **23**, 2076.

8 L. F. Hu, L. M. Wu, M. Y. Liao and X. S. Fang, *Adv. Mater*., 2011, **23**, 1988.

9 N. J. Curro, B. L. Young, J. Schmalian and D. Pines, *Phys. Rev. B*, 2004, **70**, 235117.

10 T. Hibino, A. Hashimoto, T. Inoue, J. I. Tokuno, S. I. Yoshida and M. Sano, *Science*, 2000, **288**, 203.

11 J. G. Liu, T. S. Zhao, R. Chen and C. W. Wong, *Electrochem.Commun*., 2005, **7**, 288.

12 H. Hemi, J. Ghouili, A. Cheriti, *Energy Convers. Manage*., 2015, **91**, 387.

13 P. Thounthonga, V. Chunkagb, P. Sethakula, S. Sikkabutc, S. Pierfederici, B. Davat, *J. Power Sources*, 2011, **196**, 313.

14 T. N. Danks, R. C. T. Slade and J. R. Varcoe, *J. Mater. Chem*., 2002, **12**, 3371.

15 H. Liu, C. Song, L. Zhang, J. Zhang, H. Wang and D. P. Wilkinson, *J. Power Sources*, 2006, **155**, 95.

16 B. K. Boggs and G. G. Botte, *Electrochim. Acta*, 2010, **55**, 5287.

17 H. Jiang, T. Zhao, J. Ma, C. Y. Yan and C. Z. Li, *Chem. Commun*., 2011, **47**, 1264.

18 A. L. M. Reddy, M. M. Shaijumon, S. R. Gowda and P. M. Ajayan, *Nano Lett*., 2009, **9**, 1002.

19 A. Pendashteh, M. S. Rahmanifar, R. B. Kanerc and M. F. Mousavi, *Chem. Comm*., 2014, **50**, 1972.

20 Q. F. Wang, J. Xu, X. F. Wang, B. Liu, X. J. Hou, G. Yu, P. Wang, D. Chen and G. Z. Shen, *ChemElectroChem*, 2014, **2**, 559.

21 S. K. Bikkarolla and P. Papakonstantinou, *J. Power Sources*, 2015, **281**, 243.

22 S. J. Shun, Z. Y. Wen, J. Jin, Y. M. Cui and Y. Lu, *Micropor. Mesopor. Mater*., 2013, **169**, 242.

23 A. G. Ebrahim, S. Behrouz, K. Ali, A. K. Yashar and R. Rahmatollah, *Powder Technol*., 2011, **10**, 045.

24 Y. Sharma, N. Sharma, G. V. Subba Rao and B. V. R. Chowdari, *J. Power Sources*, 2007, **173**, 495.

25 X. Wu and K. Scott, *J. Mater. Chem*., 2011, **21**, 12344.

26 M. J. Deng, C. C. Wang, P. J. Ho, C. M. Lin, J. M. Chen and K. T. Lu, *J. Mater. Chem. A*, 2014, **2**, 12857.

27 W. Xiong, M. X. Liu, L. H. Gan, Y. K. Lv, Y. Li, L. Yang, Z. J. Xu, Z. X. Hao, H. L. Liu and L. W. Chen, *J. Power Sources*, 2011, **196**, 10461.

28 D. Grosso, G. Illia, E. L. Crepaldi, B. Charleux and C. Sanchez, *Adv. Funct. Mater*., 2003, **13**, 37.

29 W. Y. Li, K. B. Xu, G. S. Song, X. Y. Zhou, R. J. Zou, J. M. Yang, Z. G. Chen and J. Q. Hu, *CrystEngComm*, 2014, **16**, 2335.

30 G. Q. Zhang, H. B. Wu, H. E. Hoster, M. B. C. Park and X. W. Lou, *Energy Environ. Sci*., 2012, **5**, 9453.

31 L. Q. Mai, F. Yang, Y. L. Zhao, X. Xu, L. Xu and Y. Z. Luo, *Nat. Commun*., 2011, **2**, 381.

32 H. W. Wang, Z. A. Hu, Y. Q. Chang, Y. L. Chen, H. Y. Wu, Z. Y. Zhang and Y. Y. Yang, *J. Mater. Chem*., 2011, **21**, 10504.

33 J. B. Cheng, Y. Lu, K. W. Qiu, D. Y. Zhang, C. L. Wang, H. L. Yan, J. Y. Xu, Y. H. Zhang, X. M. Liu and Y. S. Luo, *CrystEngComm*, 2014, **16**, 9735.

34 A. Laheäär, A. Jänes and E. Lust, *Electrochim. Acta*, 2012, **82**, 309.

35 B. Zhang, Y. Liu, Z. D. Huang, S. W. Oh, Y. Yu, Y. W. Mai and J. K. Kim, *J. Mater. Chem.*, 2012, **22**, 12133.

36 N. Spinner and W. E. Mustain, *Electrochim. Acta*, 2011, **56**, 5656.

37 H. Heli and H. Yadegari, *Electrochim. Acta*, 2010, **55**, 2139.

38 R. Ding, L. Qi, M. J. Jia and H. Y. Wang, *Catal. Sci. Technol*., 2013, **3**, 3207.

39 Y. P. Gan, H. Huang and W. K. Zhang, *Trans. Nonferrous Met. Soc*., 2007, **17**, 214.

40 S. S. Mahapatra, A. Dutta and J. Datta, *Int. J. Hydrogen Energy*, 2011, **36**, 14873.

41 H. W. Wang, J. Du, Z. Q. Yao, R. R. Yue, C. Y. Zhai, F. X. Jiang, Y. K. Du, C. Y. Wang and P. Yang, *Colloids Surf. A*, 2013, **436**, 57.

Figures

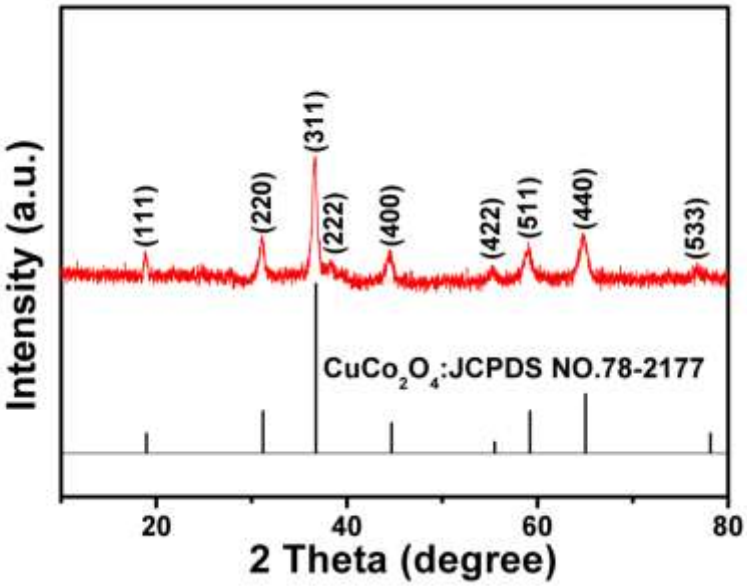

Fig. 1 XRD pattern of $CuCo_2O_4$.

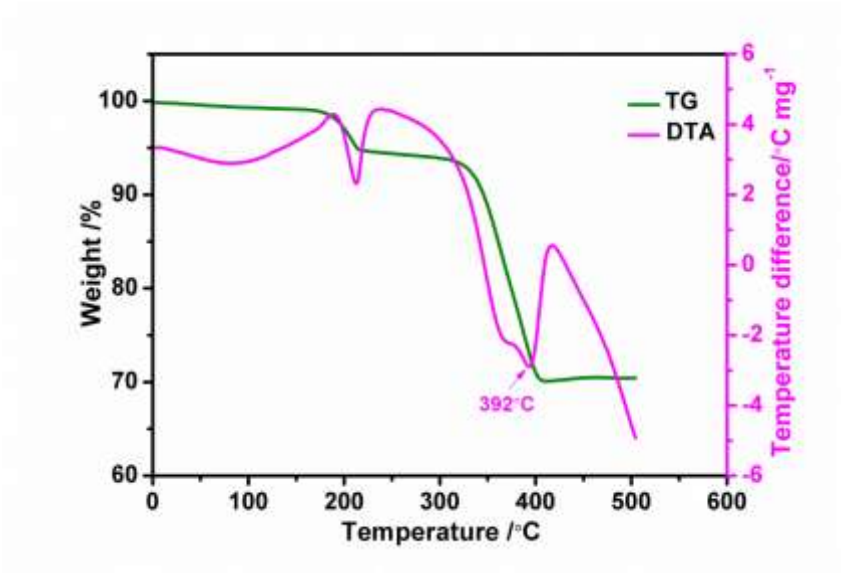

Fig. 2 TG and DTA curves of the Cu-Co hydroxide precursor after hydrothermal synthesis and before calcination.

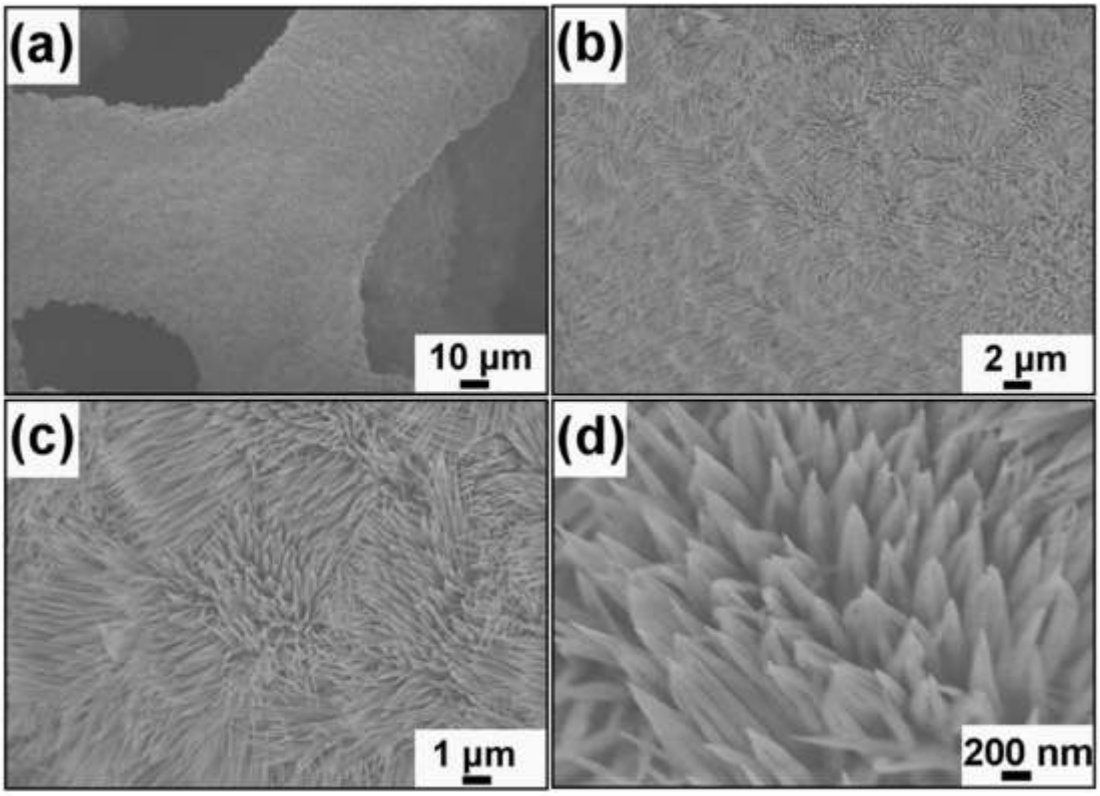

Fig. 3 (a-d) Low- and high-magnification SEM images of nanograss-shaped $CuCo_2O_4$ grown on Cu foam.

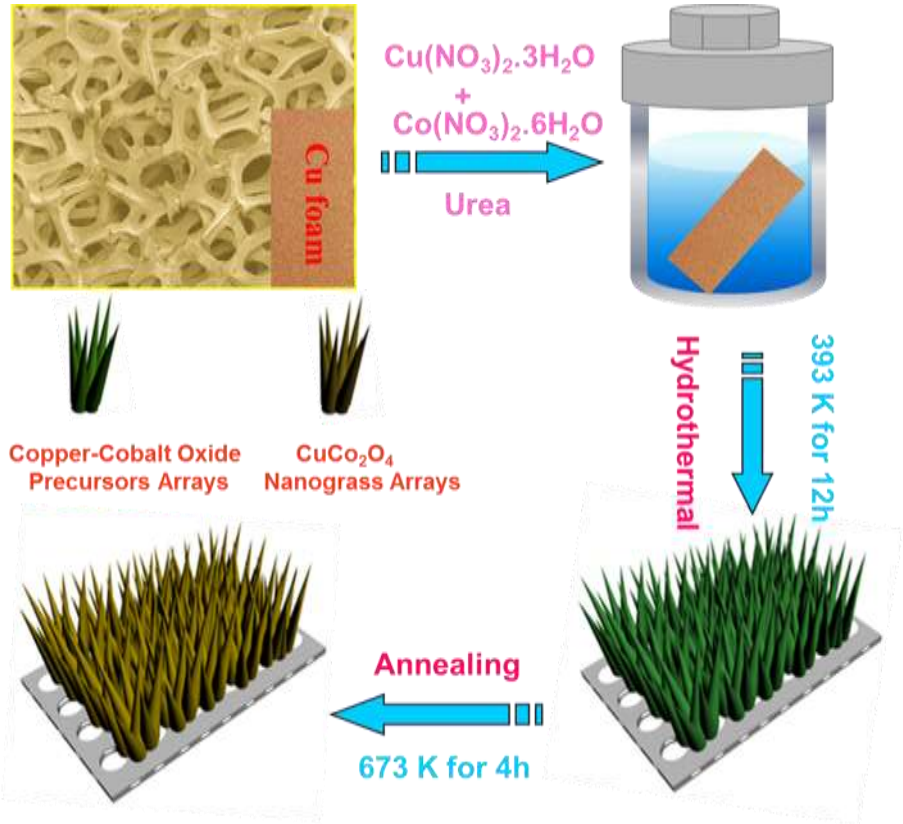

Fig. 4 Schematic illustrating the fabrication processes of $CuCo_2O_4$ nanograss.

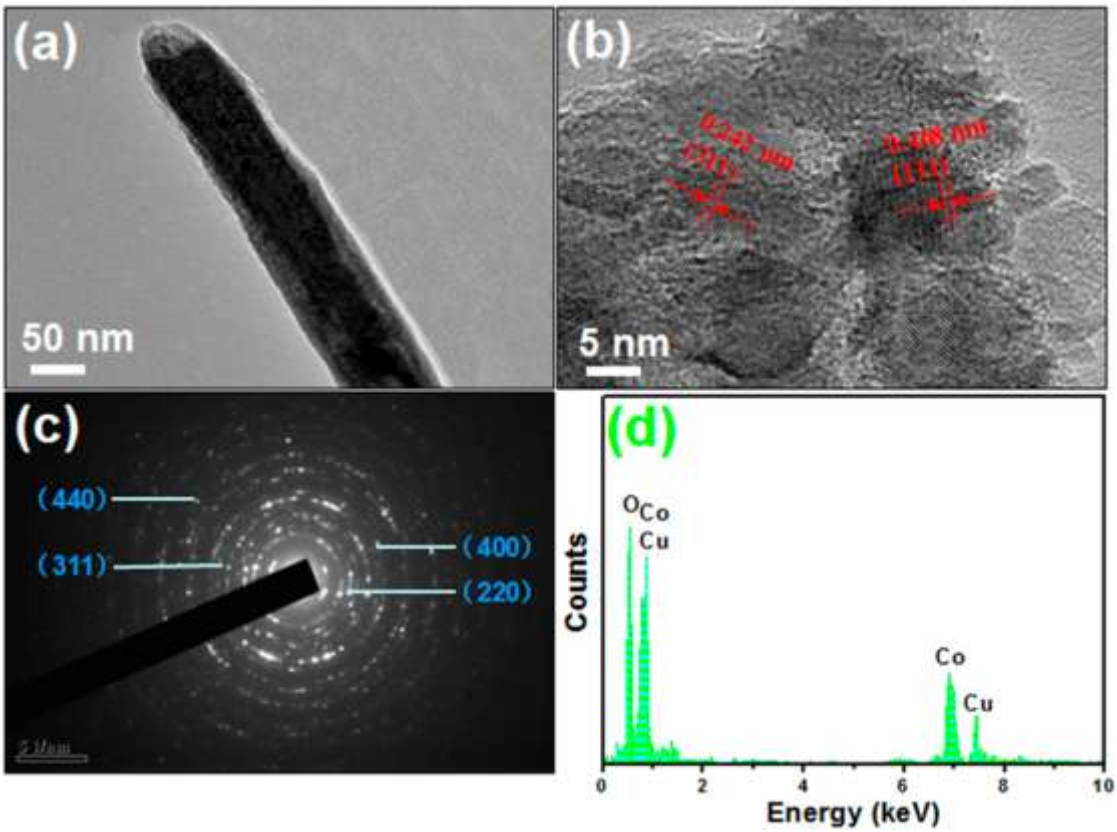

Fig. 5 (a, b) Low-magnification and high-magnification TEM images of an acicular $CuCo_2O_4$ nanograss leaf; (c) corresponding SAED pattern; and (d) energy-dispersive X-ray spectrum of the elements Co, Cu and O.

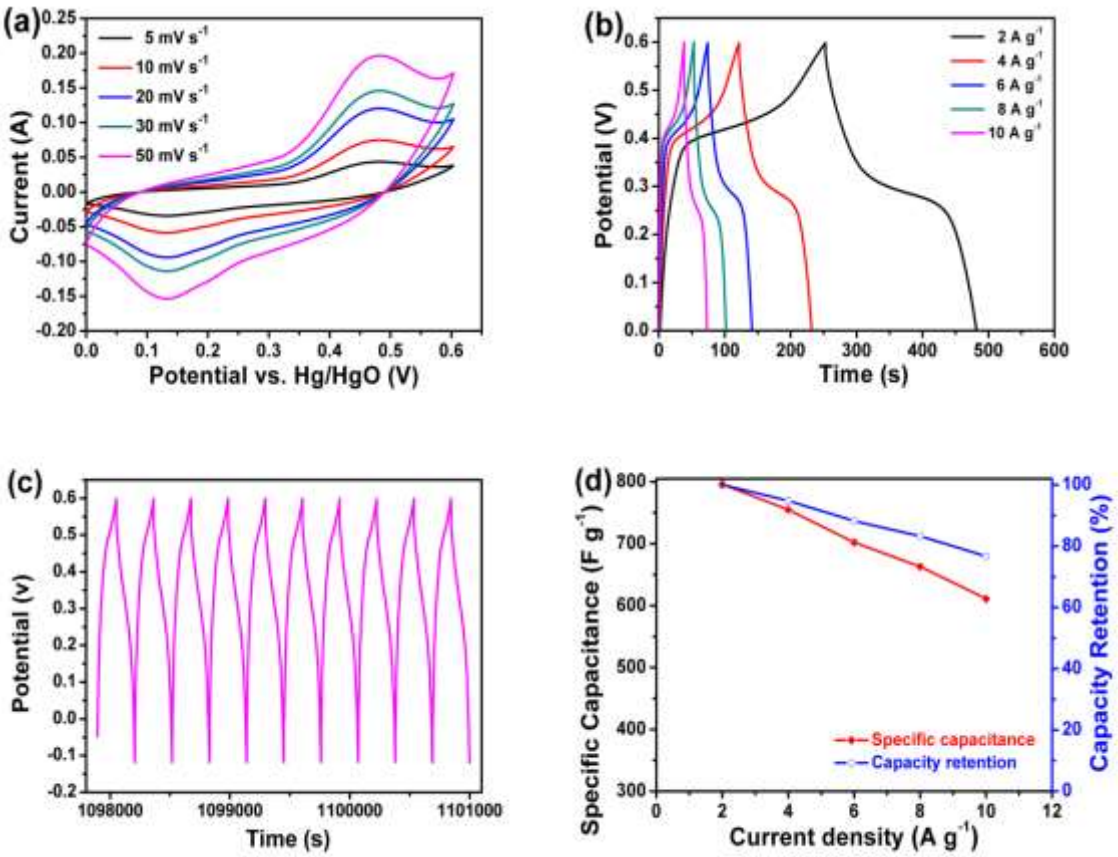

Fig. 6 (a) CV curves of the $CuCo_2O_4$ electrode at different scan rates; (b) galvanostatic discharge curves of the $CuCo_2O_4$ electrode at different current densities; (c) charge/discharge curves of the last 10 cycles among 5000 cycles; and (d) specific capacitances of the $CuCo_2O_4$ electrode as a function of current density.

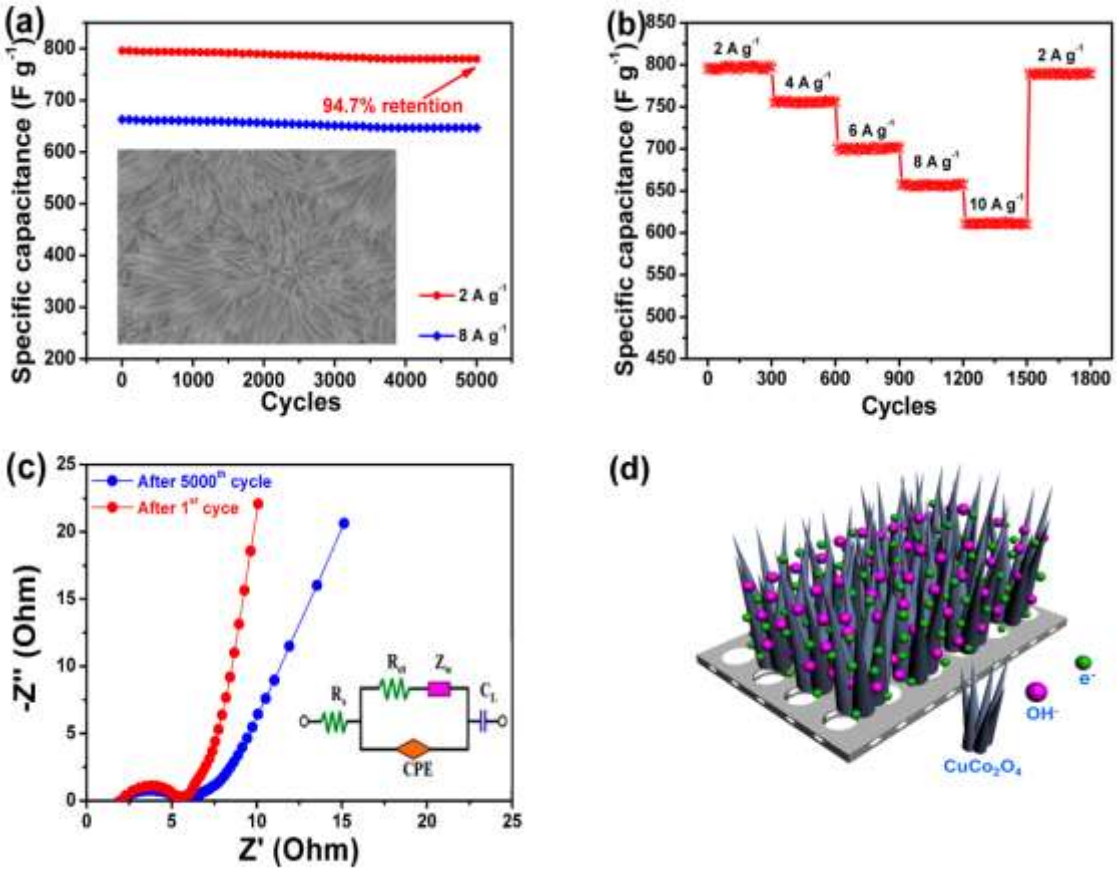

Fig. 7 (a) Cycling performance of the $CuCo_2O_4$ electrode at current densities of 2 A g^{-1} and 8 A g^{-1} and SEM image taken after 5000 cycles at 2 A g^{-1} (inset); (b) cycling stability of the $CuCo_2O_4$ at step-wisely increased current densities; (c) Nyquist plots of the $CuCo_2O_4$ electrode and equivalent circuit (inset); and (d) schematic representation of rechargeable supercapacitive electrode made from $CuCo_2O_4$ nanograss on Cu foam.

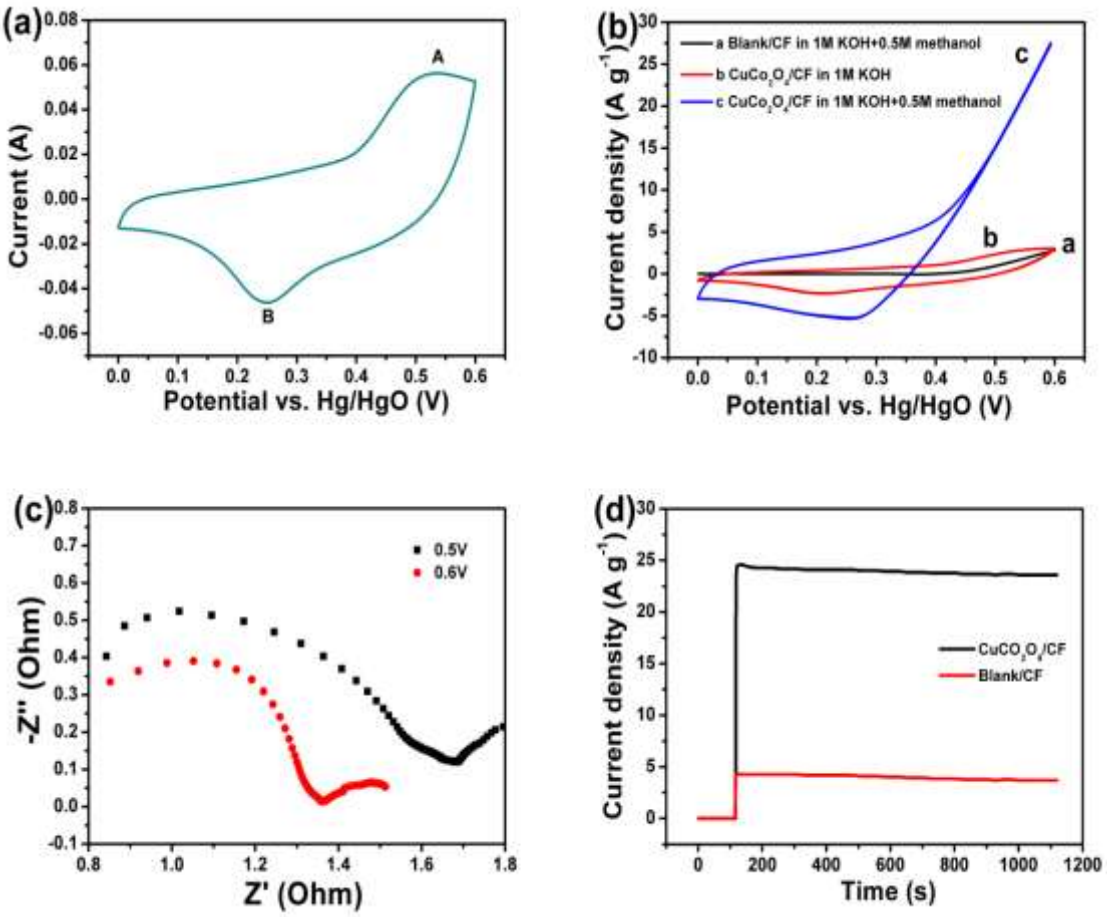

Fig. 8 (a) CV plot in 1 M KOH electrolyte at 5 mV s^{-1}; (b) CV curves of $CuCo_2O_4$/CF in 1 M KOH without (curve b) and with (curve c) 0.5 M methanol and Blank/CF in 1 M KOH with 0.5 M methanol (curve a) at a scan rate of 10 mV s^{-1}; (c) EIS plots of $CuCo_2O_4$/CF electrode in 1 M KOH with 0.5 M methanol at 0.5 and 0.6 V; and (d) CA curves of Blank/CF and $CuCo_2O_4$/CF electrodes in 1 M KOH with 0.5 M methanol at 0 V (0-120 s) and 0.6 V (120-1120 s).

Graphical Abstract

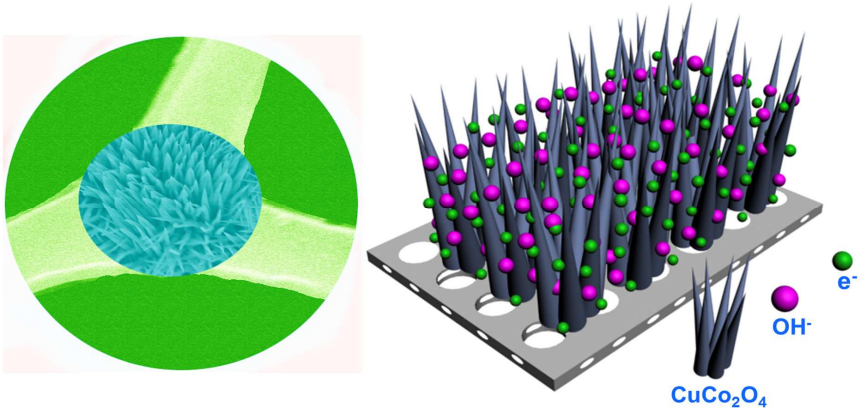

Freestanding mesoporous $CuCo_2O_4$ nanograss electrode exhibits a superior pseudocapacitive performance and a high electrocatalytic activity towards methanol oxidation.